ARCHIVES
of
FOUNDRY ENGINEERING

10.24425/afe.2026.157965

Published quarterly as the organ of the Foundry Commission of the Polish Academy of Sciences

ISSN (2299-2944)
Volume 2026
Issue 1/2026

13 – 26

2/1

Numerical Simulation and Optimization of Coke Oven Gas-Lanced Ladle Baking Process with Pure Oxygen Staged Combustion

Deng gao Chen, Guang qiang Liu *, Xin yi Cong, Ru Zeng
University of Science and Technology Liaoning, School of Civil Engineering, China
* Corresponding author: E-mail address: lgqiang0305@sina.com

Received 03.07.2025; accepted in revised form 09.09.2025; available online 27.02.2026

Abstract

To enhance the stability of the flame structure and elevate the overall combustion temperature during the staged combustion process, this study undertakes an optimization of the technology, specifically tailoring it to the context of the steel ladle baking process. Leveraging computational fluid dynamics (CFD) numerical simulation, the research conducts a thorough examination of the effects of varying ratios of primary and secondary oxygen supply on the steel ladle baking process. This examination is then juxtaposed with the conventional pure oxygen-assisted steel ladle baking process for a comparative analysis. The study reveals that, when the oxygen supply ratio for staged combustion is set at 3:7, the overall temperature within the steel ladle furnace can surpass 1500 K, aligning with the temperature achieved in the pure oxygen-assisted combustion process. This represents a notable advancement when compared to the temperatures attained with the 2:8 and 1:9 ratios. At a temperature of 1400 K, the flame exhibits a thick, rigid appearance, accompanied by a diminished area of swirling. The axial flow velocity at its core reaches 21 m/s, while the bottom impact velocity measures 8.5 m/s, both of which contribute to an enhanced convective heat transfer process. The average temperature of the steel ladle's inner wall surpasses that of the pure oxygen-assisted combustion process by 134.1 K, exhibiting a more gradual temperature gradient. Notably, the temperature discrepancy at the bottom decreases by 265.5 K, while the heating rate diminishes by 18.6%. The NOx concentration is reduced by 45%-49% compared to pure oxygen-assisted combustion. These findings provide theoretical support for energy-saving, emission reduction in the steel ladle baking process and the industrial application of staged combustion technology.

Keywords: Pure oxygen staged combustion, Pure oxygen combustion, Numerical simulation ladle baking

1. Introduction

The steel industry, recognized as a prototypical high-energy-consuming sector, constitutes an impressive 8% of the entire global energy demand. Within this industry, the steel ladle stands as a pivotal piece of thermal equipment in the metallurgical refining process. Its operational efficiency holds direct implications for the stability of the production system as well as the quality of the final products [1].

By improving the lining temperature through the steel ladle baking and preheating process, the steel pouring temperature can be effectively stabilized, reducing the risk of steel leakage during casting, while also enhancing the metallurgical quality of continuous casting billets. The optimization and innovation of the steel ladle baking process have become an important technological pathway for promoting the green and low-carbon transformation of the steel industry. Achieving the required process temperature standards while maximizing energy utilization efficiency and minimizing the emission of harmful gases such as nitrogen oxides is currently the key goal of steel ladle baking [2].

Staged combustion technology optimizes the distribution ratio of combustion gases, promoting the complete combustion of fuel. This can improve flame temperature stability and reduce the generation of pollutants [3]. Many scholars have conducted multidimensional research on this technology. In the field of boiler applications, Wang et al. simulated the operation process of a coal-fired boiler and found that multi-stage staged combustion can reduce NO_x emissions [4]; Munir et al. combined staged combustion with biomass residue and coal co-firing technology, significantly improving biomass combustion efficiency and enhancing NO_x control [5]; Zhang et al. established a three-dimensional transient model and confirmed that air-staged combustion technology made the flow field and temperature distribution in the boiler more uniform, effectively reducing the generation of fuel-based NO_x [6]. In the coke oven heating system, Jakub Poraj et al. conducted a numerical simulation combining air-staged combustion technology with the coke oven heating system and concluded that this technology could reduce NO_x emissions by more than 30%, with an optimal air ratio further reducing NOx generation [7]; Hu et al. studied air-staged combustion in vertical heating flues of coke ovens and determined that a 3:7 inlet distribution ratio resulted in the best combustion performance, with a more uniform temperature distribution and effective control of NO_x generation [8]. In comparative studies, Fan et al. compared air-staged combustion with oxygen-enriched staged combustion and found that oxygen-enriched staged combustion could more effectively reduce NO_x generation, with NO_x levels decreasing as the oxygen concentration increased [9]; experiments by MATĚJ V et al. also showed that oxygen-enriched staged combustion could reduce NO_x emissions, improve fuel combustion rates, and make the temperature distribution within the combustion zone more uniform [10].

It is evident that by adjusting the primary/secondary combustion gas ratios, combustion uniformity can be improved, temperature fluctuations can be reduced, and significant NO_x emissions reduction can be achieved, providing important references for the development of clean combustion technology. However, pure oxygen staged combustion technology has not yet been effectively applied in the steel ladle baking process. This study, based on a 100-ton steel ladle 3D model, uses computational fluid dynamics (CFD) to systematically investigate the combustion characteristics of pure oxygen staged combustion in steel ladle baking under different air supply ratios. By optimizing the primary and secondary oxygen supply ratios, the study focuses on analyzing the effects of different air supply ratios between pure oxygen combustion and pure oxygen staged combustion on the temperature field, flow field, lining temperature variation, and NO_x generation within the steel ladle furnace. The aim is to provide a theoretical basis for optimizing the steel ladle baking process, achieving a synergistic improvement in baking efficiency and energy-saving emissions reduction, and advancing the steel ladle baking process towards a green, low-carbon direction.

2. Model Establishment

2.1. Mathematical Model

The combustion process involves complex interactions of heat transfer, flow, mass transfer, and chemical reactions. Therefore, it is necessary to establish the momentum equation, energy equation, continuity equation, and species transport model to describe the combustion process in the combustion zone of the steel ladle. At the same time, the standard k-ε turbulence model is used to analyze the flow characteristics of the combustion zone. Radiative heat transfer is one of the main modes of heat exchange within the combustion zone, and the P-1 radiation model is used in this study. The specific detailed equations are as follows:

Momentum Equation [11]:

$$\frac{\partial(\rho v_i)}{\partial t} + \mathrm{div}(\rho v v_i) = -\frac{\partial}{\partial x_i}(p\delta_{ij}) + \frac{\partial}{\partial x_j}(2\mu s_{ij}) + \rho F_i \tag{1}$$

Energy Equation

$$\frac{\partial}{\partial t}(\rho T) + \mathrm{div}(\rho vT) = \mathrm{div}\left(\frac{k}{c_p}\mathrm{grad}T\right) + \frac{S_T}{c_p} \tag{2}$$

Continuity Equation

$$\frac{\partial}{\partial t}(\rho T) + \mathrm{div}(\rho vT) = \mathrm{div}\left(\frac{k}{c_p}\mathrm{grad}T\right) + \frac{S_T}{c_p} \tag{3}$$

In equations (1-3): ρ is the density; t is time; v is velocity; v_i is the velocity in the i-th direction; p is the fluid pressure; δ_ij is the stress tensor; x_i, x_j are directional tensors; μ is the turbulence viscosity; F_i is the unit mass force in the i-th direction; T is the thermodynamic temperature; k is the thermal conductivity of the fluid; c_p is the specific heat capacity of the fluid at constant pressure; grad(T) is the thermodynamic temperature gradient; S_T is the heat source term per unit volume.

The turbulence model uses the standard k-ε model [12]:

$$\begin{aligned}\rho\frac{dk}{dt} = \rho\left(\frac{\partial k}{\partial t} + \mu_j\frac{\partial k}{\partial x_j}\right) = \frac{\partial}{\partial x_j}\left[\left(\mu + \frac{\mu_t}{\sigma_k}\right)\frac{\partial k}{\partial x_j}\right] \\ + \mu_i\frac{\partial\mu_i}{\partial x_i}\left(\frac{\partial\mu_i}{\partial x_j} + \frac{\partial\mu_j}{\partial x_j}\right) - \rho\varepsilon\end{aligned} \tag{4}$$

$$\begin{aligned}\varepsilon\rho\frac{dk}{dt} = \rho\left(\frac{\partial\varepsilon}{\partial t} + \mu_j\frac{\partial\varepsilon}{\partial x_j}\right) = \frac{\partial}{\partial x_j}\left[\left(\mu + \frac{\mu_t}{\sigma_\varepsilon}\right)\frac{\partial\varepsilon}{\partial x_j}\right] \\ + \frac{c_1\varepsilon}{k}\mu_i\frac{\partial\mu_i}{\partial x_i}\left(\frac{\partial\mu_i}{\partial x_j} + \frac{\partial\mu_j}{\partial x_j}\right) - c_2\rho\frac{\varepsilon^2}{k}\end{aligned} \tag{5}$$

In equations (4-5): ρ is the density; k is the turbulent kinetic energy; μ is the dynamic viscosity of the fluid; μ_t is the turbulence viscosity; u_i,u_j are the directional velocities of the fluid; x_i, x_j are the directional tensors; σ_k is the Prandtl number for turbulent kinetic energy k; ε is the turbulent kinetic energy dissipation rate; σ_ε is the effective Prandtl number for the turbulent kinetic energy dissipation rate; c_1, c_2 are empirical constants.

This study pertains to non-premixed gas combustion, and the turbulent dissipation model is used to describe the chemical reaction rate throughout the combustion process. This model assumes that the reaction rate is controlled by the turbulence model, avoiding the complexity of chemical kinetics calculations and achieving the goal of simplifying the computations. The turbulent dissipation equation is shown in Equation (6) [13].

$$R_{ri} = \upsilon'_{w,r} A \rho \frac{\varepsilon}{k} \min_R \left(\frac{Y_R}{\upsilon'_{R,r} M_{w,R}} \right) \tag{6}$$

In equation (6): R_{ri} is the vortex dissipation reaction rate; $\upsilon'_{w,r}$ represents the stoichiometric coefficient of w in reaction r; A is an empirical constant, A = 4.0; ρ is the density; ε is the turbulent kinetic energy dissipation rate; k is the turbulent kinetic energy; $\min_R$ represents the minimum value of reactant R; $\upsilon'_{R,r}$ represents the stoichiometric coefficient of R in reaction r; Y_R is the mass fraction of the reactant; $M_{w,R}$ is the molecular weight of component R.

The combustion model uses the P-1 radiation model, as shown in Equation (7) [14]:

$$\begin{aligned} &\frac{dI(r,\overrightarrow{s})}{dx} + (a + \sigma_s) I(\vec{r},\vec{s}) = an^2 \frac{\sigma T^4}{\pi} \\ &+ \frac{\sigma_s}{4\pi} \int_0^{4\pi} I(\vec{r},\vec{s}) \Phi(\vec{s},\vec{s}') d\Omega' \end{aligned} \tag{7}$$

In equation (7): I is the radiation intensity; $\vec{s}$ is the direction vector; $\vec{r}$ is the position vector; x is the coordinate in the radiation propagation direction; a is the absorption coefficient; n is the refractive index of the medium; σ_s is the scattering coefficient; σ is the Stefan-Boltzmann constant, which is 5.672 × 10-8 W/(m^2 • K^4); $\Phi(\vec{s}, \vec{s}')$ is the scattering phase function, which describes the probability distribution of radiation scattering from direction s to direction $\vec{s}'$; $d\Omega'$ is the differential solid angle.

The formation of NOx during the combustion process mainly includes thermal, prompt, and fuel-based types, which are controlled by Reaction (8) and Reaction (9) [15].

$$NO_2 \overset{CO}{\rightarrow} 2NO \tag{8}$$

$$N_2 + O_2 \rightarrow 2NO \tag{9}$$

$$\phi(NO) = \frac{\chi_{(NO)} \times 10^6}{1 - \chi_{(H_2O)}} \tag{10}$$

Define a new variable $\phi(NO)$ as the measured NO molar concentration, and its calculation formula is shown in Equation (10).

In equation (10): $\chi_{(NO)}$ is the molar fraction of NO; $\chi_{(H_2O)}$ is the molar fraction of H_2O.

To ensure the accuracy of the simulated fuel combustion data, the results use the improved Weighted Sum Gray Gas Absorption Model (WSGGM) [16].

2.2. Physical Model

This study takes a 100-ton steel ladle from a certain company as the object of research. The steel ladle is simplified as a cylinder with a height of 3285 mm and a lid diameter of 2430 mm. The interior of the steel ladle is the combustion zone, with a bottom diameter of 2200 mm and a top diameter of 2420 mm. The steel ladle wall is divided into three layers: the thermal insulation layer, the permanent layer, and the working layer, as shown in Figure 1(a). The physical property parameters of the refractory material of the steel ladle wall are detailed in Table 1. A monitoring point d1 is set at the center of the bottom of the steel ladle, Monitoring points d2Б d3Б d4 and d5 are set at the steel ladle inner wall at Y=385 mm, Y=1351.6 mm, Y=2318.4 mm, and Y=3185 mm, respectively, to observe the temperature variation process of the steel ladle inner wall.

The burner and combustion air inlet are velocity inlets, and the fuel inlet is coke oven gas with a flow rate of 625 m^3/h. The specific composition is shown in Table 2. When using staged combustion technology, pure oxygen is chosen as the combustion air. The primary oxygen (O1) and secondary oxygen (O2) air supply ratios are 3:7, 2:8, and 1:9. The velocity boundary conditions are shown in Table 3. The flue gas outlet is a pressure outlet. The heat from the combustion zone is transferred outward through the steel ladle's insulation layer, with a heat transfer coefficient of 8 W/(m^2 • K) [17].

The mesh structure is shown in Figure 1(c). The physical model is established using SpaceClaim, and unstructured mesh division is carried out using Fluent Meshing. After model validation, it was determined that a medium grid (483,300 cells) should be used for numerical calculations.

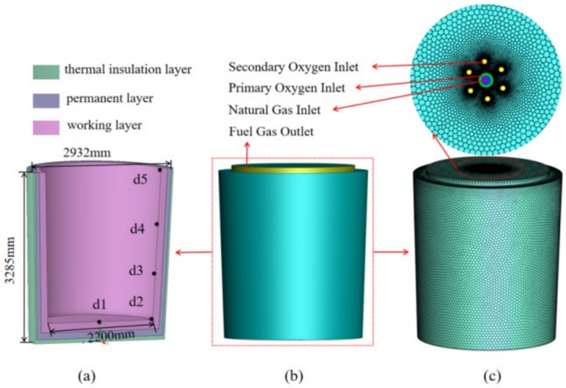

Fig. 1. (a) Schematic diagram of the ladle structure;(b) Ladle calculation model;(c) ladle mesh generation model

Table 1.
Physical property parameters of refractory materials

Hierarchy	Material	Steel ladle wall thickness (mm)	Steel ladle bottom thickness (mm)	Density (kg/m^3)	Specific heat capacity (J/(kg·K))	Thermal conductivity (W/(kg·K))
Steel ladle shell	SM490B	36	75	7380	480	56
Permanent layer	High-alumina brick	85	130	2380	857	1.22
Working layer	Magnesia-carbon brick	135	180	2900	780	2.1

Table 2.
Composition of natural gas

Composition	CH_4	C_2H_4	C_2H_6	C_3H_6	CO_2	N_2	H_2	O_2	CO
Volume fraction (%)	29.65	4.21	2.76	2.2	1,93	2.16	50.47	0.32	1.93

Table 3.
Velocity boundary condition

-	Scheme	O_1:O_2=3:7	O_1:O_2=2:8	O_1:O_2=1:9	Non-staged combustion
Different secondary oxygen velocities	Primary oxygen (O_1) velocity (m/s)	7.68	7.68	7.68	14.78
	Secondary oxygen (O_2) velocity (m/s)	14.78	17.08	19.20	
Different primary oxygen velocities	Primary oxygen (O_1) velocity (m/s)	7.68	5.12	2.55	
	Secondary oxygen (O_2) velocity (m/s)	14.78	14.78	14.78	

2.3. Model Validation

To ensure the reliability of the numerical simulation results, this study carried out a grid independence verification. A three-level grid refinement scheme was used for the analysis: the base grid (scheme a) consists of 414,800 cells; the medium grid (scheme b) consists of 483,300 cells; and the fine grid (scheme c) consists of 568,200 cells. By analyzing the temperature variations at each monitoring point inside the steel ladle when O_1:O_2=3:7 (Figure 2), it was found that: the temperature gradient distribution between the base grid and the medium grid shows a significant difference, with the maximum relative temperature difference Δt=102.35 K (deviation > 5%). The temperature gradient variations between the medium grid and the fine grid tend to align [18].

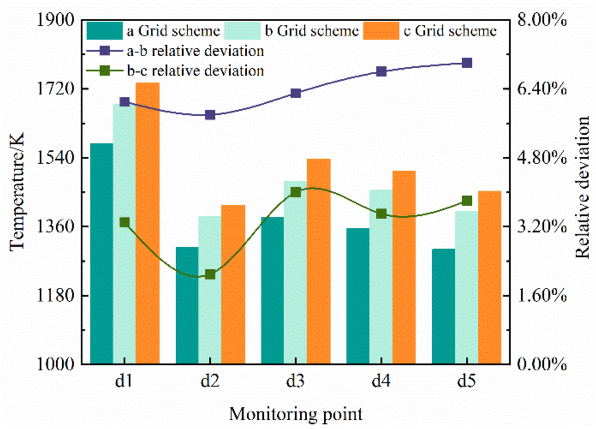

Fig. 2. Grid Independence Verification

3. Results and Discussion

3.1. The effect of secondary air velocity on the baking performance under different air supply ratios

1) The effect of secondary air velocity on the flow field inside the ladle

The gas flow state inside the steel ladle is an important factor affecting the temperature uniformity of the ladle and is also a challenging aspect of the steel ladle baking process [11]. The coke oven gas and combustion air form a high-speed jet through the burner and enter the furnace. The entire combustion zone flow field is in a turbulent state, with the flow field structure distribution shown in Figure 3. Observing the Z=0 mm cross-section, the initial velocity gradient of the jet shows a typical symmetric distribution along the central axis throughout the process. The high-temperature flue gas generated by combustion impacts the steel ladle bottom and, after being constrained by the refractory lining, undergoes radial diffusion and rises along the ladle wall to form a vortex region [19, 20]. The fluid velocity near the wall in the vortex region increases radially, and due to viscous effects, the velocity in the rising stage along the ladle wall decreases, reaching a minimum at the flue gas outlet. The size of the vortex region affects the circulation speed of the high-temperature flue gas. Observing the velocity contours at the bottom of the steel ladle, it can be seen that under the O_1:O_2=2:8 process, the vortex region area is the largest, causing the impact velocity of the high-temperature flue gas on the steel ladle bottom to be the smallest. In comparison, the vortex region area is effectively controlled under the O_1:O_2=3:7 process, allowing the high-temperature flue gas to quickly collide with the steel ladle bottom, accelerating the flow turning efficiency, increasing the circulation speed of the high-temperature flue gas, and enhancing heat transfer efficiency.

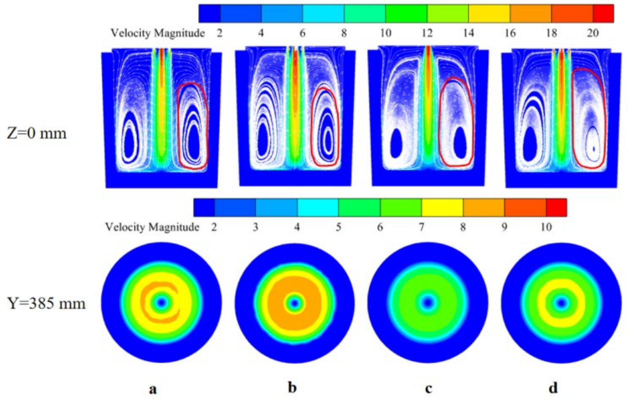

Fig. 3. Flow field distributions of different sections. a:Pure oxygen combustion support; b:O_1:O_2=3:7; c:O_1:O_2=2:8; d:O_1:O_2=1:9

To gain a deeper understanding of the impact of the vortex region on the flow field at the base of the steel ladle, this study extracts and compares the variations in velocity at various time points, ranging from the center of the steel ladle's bottom to its wall. These comparisons are illustrated in Figure 4. The results indicate that, across all four processes, the velocity exhibits a trend of initial increase followed by a decrease as it moves from the center of the steel ladle's bottom towards its wall. In proximity to the juncture of the steel ladle bottom and its lining, the velocity undergoes a gradual decrement. This decrement is attributable to the obstruction of gas flow at the interface between these two walls, ultimately giving rise to a recirculation dead zone. Since the vortex region area is effectively controlled, when O_1:O_2=3:7, the velocity of the high-temperature flue gas impacting the steel ladle bottom is the highest, with the maximum velocity difference from the edge region reaching 8.88 m/s, which enhances the heat transfer effect under this process. Compared to pure oxygen combustion, O_1:O_2=2:8, and O_1:O_2=1:9 processes, the maximum flow velocity at 0.4 m under the O_1:O_2=3:7 process increased by 11.8%, 36.4%, and 24.8%, respectively. The significant increase in the high-temperature flue gas velocity maximizes the heat transfer efficiency inside the steel ladle, compensating for the shortcomings of pure oxygen staged combustion in heat transfer.

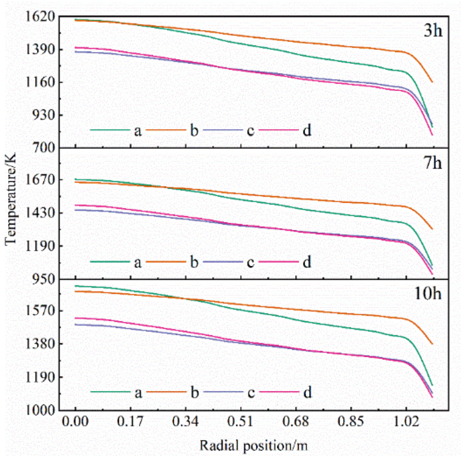

Fig. 4. Velocity distributions at the bottom of the ladle .a:Pure oxygen combustion support; b:O_1:O_2=3:7; c:O_1:O_2=2:8; d:O_1:O_2=1:9

2) The effect of secondary air velocity on flame morphology

To delve deeper into the temperature distribution characteristics within the steel ladle, this study undertakes a comparative analysis of the flame state at the 1400 K isothermal surface flame temperature across four distinct processes. This comparison is visually represented in Figure 5. Upon observation, it becomes evident that as time elapses, the stability of the combustion flame structure undergoes a gradual enhancement. Specifically, examining the flame state at the 10th hour under the pure oxygen combustion process, the flame width attains a measurement of 458.3 mm. However, it is noteworthy that disruptions in the high-temperature flame are evident at the points of fuel and oxygen inlet. When employing the ratio of O_1:O_2=3:7, the flame width expanded to 534.7 mm, marking a 16.7% increase. Conversely, ratio of O_1:O_2 is 2:8 and 1:9, the flame widths decreased by 16.7% and 25%, respectively, in comparison to the pure oxygen combustion process. Conclusively, the ratio of O_1:O_2=3:7 enhances the stability of the combustion flame structure, thereby guaranteeing a uniform temperature increase within the steel ladle and preventing the occurrence of large temperature discrepancies. Furthermore, the ratio of O_1:O_2 is 2:8 and 1:9, influenced by the flame structure, exhibited considerable flame disruptions across substantial areas, ultimately resulting in subpar heat transfer efficiency.

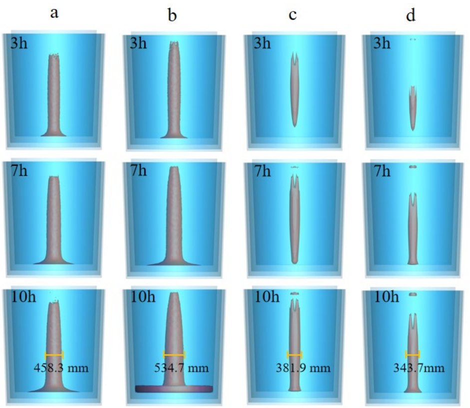

Fig. 5. Flame shape structure at 1400 K. a:Pure oxygen combustion support; b:O_1:O_2=3:7; c:O_1:O_2=2:8; d:O_1:O_2=1:9

3) The effect of secondary air velocity on the ladle temperature field

The primary task of the steel ladle baking process is to quickly, stably, and uniformly heat the ladle to the target temperature [21]. Figure 6 shows the temperature distribution at the center cross-section of the ladle at six different times. Under all four processes, the temperature of the ladle gradually increased as the baking time progressed, and by the end of the baking process, the temperature reached 1500 K, meeting the temperature requirements for steel ladle baking. By observing the temperature distribution under staged combustion processes, it can be seen that as the secondary air velocity increases, the area with temperatures greater than 1600 K gradually decreases. Comparing the pure oxygen combustion process and the O_1:O_2=3:7 process, at the end of the baking process, the temperature distribution within the ladle for both processes is nearly identical. However, for the O_1:O_2=2:8 and O_1:O_2=1:9 processes, the temperature within the ladle is significantly lower than that of the pure oxygen combustion and O_1:O_2=3:7 processes. This further verifies the previous discussion regarding how the flame structure and the internal flow field of the ladle affect heat transfer.

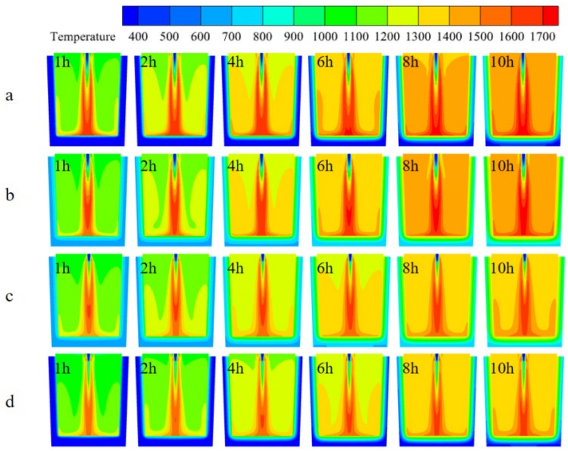

Fig. 6. Temperature field in the ladle. a:Pure oxygen combustion support; b:O_1:O_2=3:7; c:O_1:O_2=2:8; d:O_1:O_2=1:9

The temperature distribution of the steel ladle lining plays a crucial role in the ladle baking process [22]. Figure 7 compares the temperature distribution on the ladle wall at different baking times under different processes, with a local magnification of the ladle wall selected for analysis. It can be observed that as baking progresses, the wall temperature for all four processes steadily increases, and by the end of the baking process, the ladle wall temperature reaches 1200 K.Through comparative analysis, it is found that the temperature rise on the ladle wall is more significant under the O_1:O_2=3:7 process, surpassing the inner wall temperature of the pure oxygen combustion process. On the other hand, the inner wall temperature for the O_1:O_2=2:8 and O_1:O_2=1:9 processes is noticeably lower than that of the pure oxygen combustion process. Particularly under the O_1:O_2=1:9 process, the inner wall temperature of the ladle reaches the minimum, further confirming the impact of the coarse flame structure under the O_1:O_2=3:7 process on heat transfer within the ladle, as discussed in Figure 5.

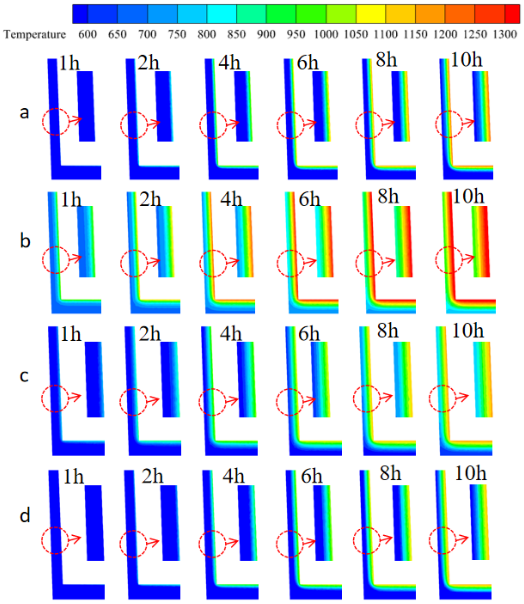

Fig. 7. Temperature distribution of the ladle wall. a:Pure oxygen combustion support; b:O_1:O_2=3:7; c:O_1:O_2=2:8; d:O_1:O_2=1:9

This paper selects four temperature monitoring points on the steel ladle inner wall (the positions of the monitoring points are marked in Figure 1) to further analyze the temperature changes on the steel ladle inner wall, as shown in Figure 8. It can be observed that under all four processes, the temperature at each monitoring point gradually increases over time, and the heating rate gradually decreases. The d5 monitoring point, located near the flue gas outlet, has the lowest temperature, as the discharge of flue gas carries away a large amount of heat, resulting in heat loss. Upon examining the three pure oxygen staged combustion processes, the temperature at the d3 monitoring point is the highest. Under the O_1:O_2=3:7 process, the temperature difference between monitoring points d3 and d5 is 78.2 K, which is 30.4% and 39% lower than the maximum temperature differences in the O_1:O_2=2:8 and O_1:O_2=1:9 processes, respectively. In contrast, under the pure oxygen combustion process, the temperature at monitoring point d2 is higher than that at the other three monitoring points. This is because the recirculation zone formed in the furnace under the pure oxygen combustion process is located relatively low, with a lesser impact on the temperature at the junction of the ladle wall and bottom. The maximum temperature difference reaches 102.9 K. By comparing the O_1:O_2=3:7 process with the pure oxygen combustion process, the maximum temperature difference between the monitoring points under the O_1:O_2=3:7 process is reduced by 24%. This demonstrates that the O_1:O_2=3:7 process results in a more uniform temperature distribution on the steel ladle inner wall, which is beneficial for extending the service life of the ladle lining.

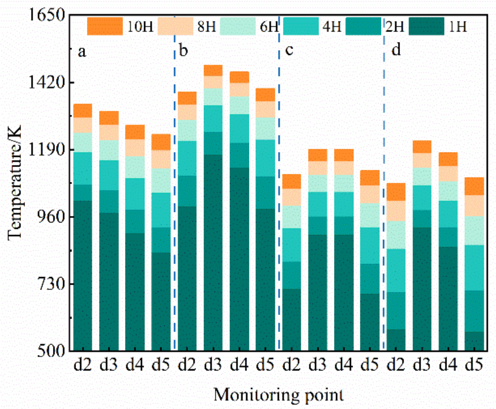

Fig. 8. Temperature changes at monitoring points. a:Pure oxygen combustion support; b:O_1:O_2=3:7; c:O_1:O_2=2:8; d:O_1:O_2=1:9

In Figure 9, it can be observed that as the baking process progresses, the bottom temperature of the steel ladle gradually increases under all four processes. The temperature of the steel ladle bottom expands from the center to the periphery in an approximately concentric manner. This is because the central area of the steel ladle bottom is directly beneath the burner, where fuel combustion is intense, continuously releasing a large amount of heat. The temperature is lowest at the junction between the steel ladle bottom and the lining wall, due to the formation of a dead zone in the flow field inside the ladle, resulting in poor heat transfer. This phenomenon further verifies the conclusions drawn from Figure 7. Upon further comparison, it can be found that as the secondary air velocity decreases, the high-temperature region at the bottom of the steel ladle increases in both size and area. The pure oxygen combustion process has the largest high-temperature area, while the O_1:O_2=3:7 process has a high-temperature area close to that of the pure oxygen combustion process, better meeting the required baking temperature for the refractory bricks at the steel ladle bottom in the baking process.

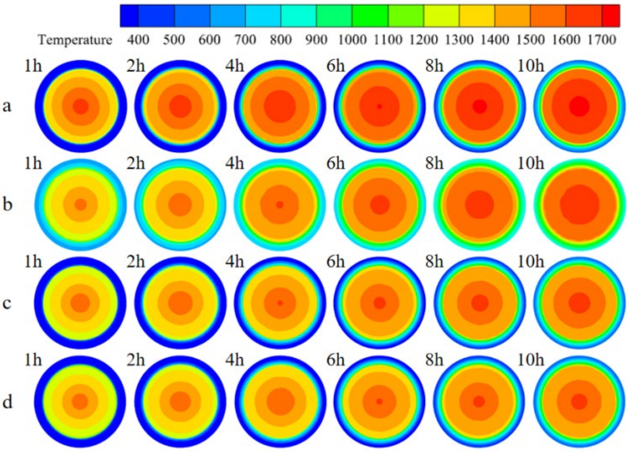

Fig. 9. Temperature nephogram at the bottom of the ladle. a:Pure oxygen combustion support; b:O_1:O_2=3:7; c:O_1:O_2=2:8; d:O_1:O_2=1:9

To better analyze the temperature variation at the bottom of the steel ladle, this study extracts the temperature from the center of the steel ladle bottom radially at three time points: 3 h, 7 h, and 10 h, as shown in Figure 10. From the analysis, it can be observed that as time progresses, the overall temperature of the steel ladle bottom increases. Since the flame formation area is located directly above the center of the steel ladle bottom, at the end of the baking process, the temperature at the center position is significantly higher than at other locations on the bottom, creating a temperature difference. In the pure oxygen combustion process, the temperature difference between the center and the edge of the ladle bottom reaches 565.4 K, which is 88.5% higher compared to the O_1:O_2=3:7 process (which has a temperature difference of 299.9 K between the center and the edge). By observing the temperature differences under the staged combustion processes, the temperature difference between the center and the edge of the steel ladle bottom is 451.5 K (for O_1:O_2=1:9), 389.7 K (for O_1:O_2=2:8), and 299.9 K (for O_1:O_2=3:7). This shows that as the secondary air velocity decreases, the temperature difference between the center and the edge of the steel ladle bottom gradually decreases, and it becomes much smaller than in the pure oxygen combustion process. This indicates that at O_1:O_2=3:7, the temperature distribution at the bottom of the steel ladle is more uniform, which helps avoid irreversible damage to the refractory bricks at the bottom due to local high temperatures.

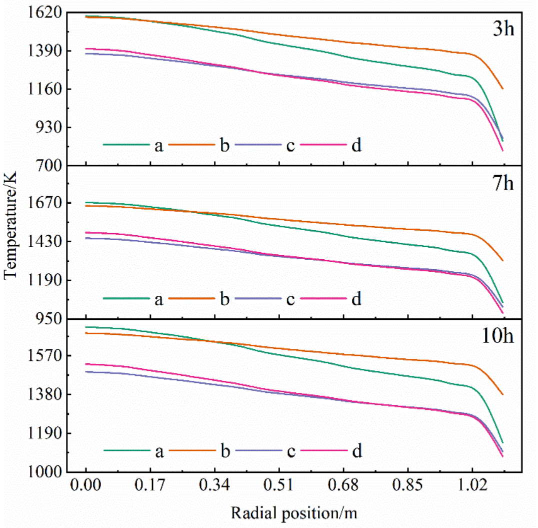

Fig. 10. Radial temperature variation at the bottom of the ladle. A:Pure oxygen combustion support; b:O_1:O_2=3:7; c:O_1:O_2=2:8; d:O_1:O_2=1:9

4) The effect of secondary air velocity on NOx concentration

The spatial distribution characteristics of nitrogen oxides (NOx) concentration at key sections of the steel ladle at the end of the baking process are shown in Figure 11 (Z=0 mm, Y=385 mm, Y=1400 mm, Y=3285 mm). Comparative analysis indicates that the NOx concentration distribution in the pure oxygen staged combustion process is significantly lower at each section than in the traditional pure oxygen combustion process. Additionally, the NOx generation increases as the first-stage oxygen supply ratio increases. Since the flame structure and combustion temperature in the O_1:O_2=3:7 process closely resemble those of the pure oxygen combustion process, the thermal NOx concentration is higher compared to other staged air ratio processes. However, it remains significantly lower than in the traditional pure oxygen combustion process. The nitrogen oxides studied in this research are primarily thermal NOx, and its generation rate mainly depends on the flame temperature, the size of the high-temperature region, and the high-temperature flue gases during the combustion process. Therefore, from the observation of Figure 11, it is evident that high concentrations of NOx are primarily concentrated around the high-temperature flames, the steel ladle bottom, and the gas outlet. Upon observing the NOx mass fraction distribution at Y=385 mm (steel ladle bottom), it can be seen that the NOx mass fraction decreases radially, as expected. Due to the swirl dead zone effect, the lowest NOx concentration occurs at the edges of the ladle bottom, with a significant difference in concentration between the center and the edges.

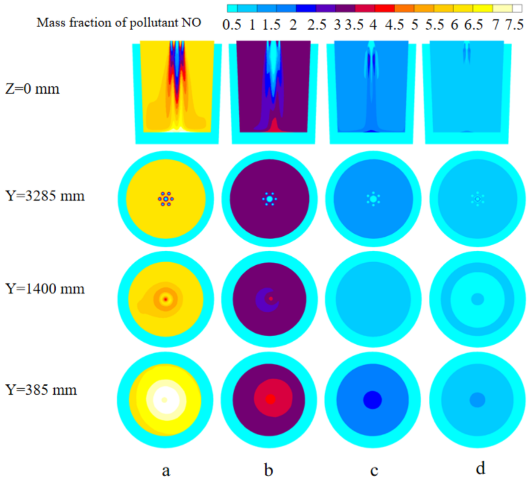

Fig. 11. NOx concentration distribution in different sections. a:Pure oxygen combustion support; b:O_1:O_2=3:7; c:O_1:O_2=2:8; d:O_1:O_2=1:9

Figure 12 reveals the distribution characteristics of NOx mass concentration fraction under different processes. It can be observed that at Y=3285 mm (gas outlet), the NOx mass concentration fluctuates significantly along the radial position. The fluctuation diminishes as the distance from the center increases, and after a radial position of 0.38 m, the NOx concentration tends to stabilize. Under the pure oxygen combustion process, the fluctuation in NOx mass fraction is the largest, with a maximum difference of 6.2, and the NOx concentration is much higher than in the other three processes. In the O_1:O_2=3:7 process, the maximum difference reaches 3.4, which is a 43.7% reduction compared to the pure oxygen combustion process. Similarly, in the analysis of NOx concentration distribution at Y=385 mm (steel ladle bottom), it can be seen that the O_1:O_2=3:7 process reduces the maximum difference in NOx concentration by 46.7% compared to the pure oxygen combustion process.

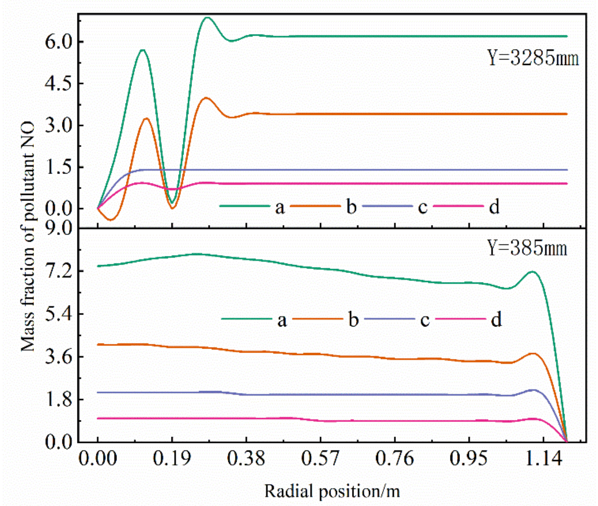

Fig. 12. Radial distribution of NOx concentration. a: Pure oxygen combustion support; b:O_1:O_2=3:7; c:O_1:O_2=2:8; d:O_1:O_2=1:9

3.2. Influence of primary air velocity on baking effect under different air supply ratios

When the secondary air velocity is kept constant, the impact of primary air velocity under different air supply ratios on the flow field, temperature field, and pollutants within the steel ladle is analyzed.

1) The impact of primary air velocity on the flow field within the ladle

Figure 13 reveals the flow field characteristics inside the furnace under different primary air velocities, pure oxygen combustion, and four staged combustion processes. Observing the flow field distribution at the Y = 385 mm interface, it can be seen that for all four processes, the velocities at the center and edge positions are the lowest, and the overall flow exhibits a change pattern of increasing first and then decreasing, following a concentric circle form. Due to the influence of the recirculation zone, the flow field distribution at the bottom of the steel ladle (Y = 385 mm) in the pure oxygen combustion process shows a velocity breakpoint. A comparative analysis of pure oxygen and staged combustion shows that under the O_1:O_2=3:7 process, the steel ladle bottom (Y = 385 mm) is subjected to the greatest impact from high-temperature flue gases, reaching 8.8 m/s. Since the O_1:O_2=3:7 process effectively reduces the area of the recirculation zone, it accelerates the convective speed of high-temperature flue gases, enhancing the heat transfer efficiency within the furnace and improving the temperature uniformity at the bottom of the steel ladle.

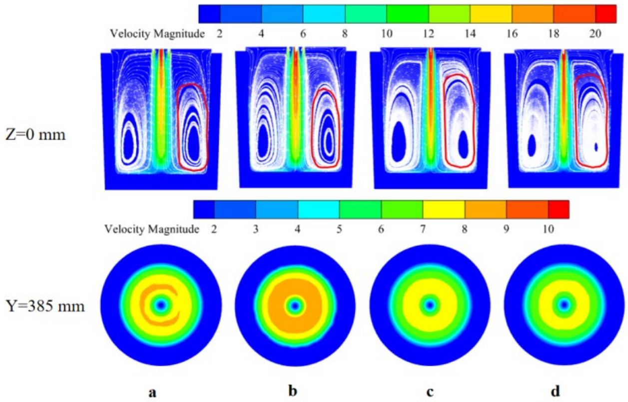

Fig. 13. Flow field distributions of different sections. a :Pure oxygen combustion support; b:O_1:O_2=3:7; c:O_1:O_2=2:8; d:O_1:O_2=1:9

Figure 14 reveals the velocity variation from the center of the steel ladle bottom to the wall at different times for three staged air supply ratios and pure oxygen combustion. The trends of high-temperature flue gas impact velocity on the steel ladle bottom at different times are consistent for all four processes. At the end of the baking process, the average impact velocity of high-temperature flue gases on the steel ladle bottom in pure oxygen combustion is 5.41 m/s. Due to the effective reduction in the recirculation zone area, the average impact velocity in the O_1:O_2 = 3:7 process increases by 10.2% compared to pure oxygen combustion. In contrast, under the O_1:O_2 = 2:8 and O_1:O_2 = 1:9 processes, the average impact velocities of high-temperature flue gases on the steel ladle bottom are 5.38 m/s and 5.21 m/s, respectively, showing a significant decrease compared to the O_1:O_2 = 3:7 process. This reduction causes the high-temperature flue gas flow speed inside the steel ladle to slow down, hindering the heat transfer within the ladle.

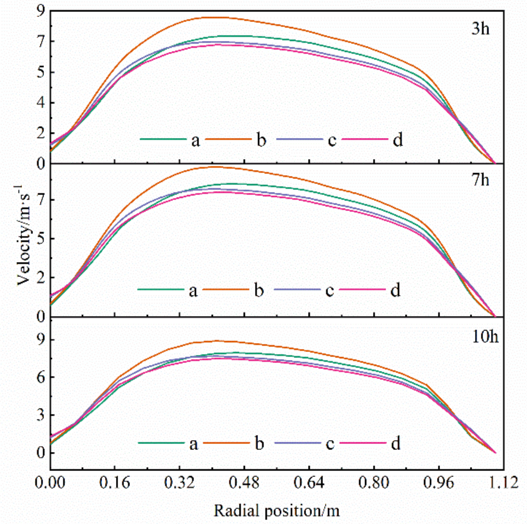

Fig. 14. Velocity distributions at the bottom of the ladle. a:Pure oxygen combustion support; b:O_1:O_2=3:7; c:O_1:O_2=2:8; d:O_1:O_2=1:9

2) The impact of primary air velocity on flame shape

To further explore the reasons behind the differences in high-temperature flame formation positions inside the steelmaking furnace, Figure 15 reveals the flame shape structure at the 1400 K isotherm under four different processes. It can be observed that during the early stages of the baking process, high-temperature flames in all four processes exhibited flame extinction phenomena. As combustion continued, the length of the flame extinction zone gradually decreased. At the end of the baking process, in the pure oxygen combustion process, due to the high-speed injection of fuel and oxygen, a local extinction zone with a length of 337.2 mm appeared at the nozzle. In the O_1:O_2 =3:7 process, a relatively stable high-temperature flame structure was formed, but a flame extinction zone of 146.6 mm was also present at the nozzle. In the O_1:O_2 =2:8 process, an unstable high-temperature flame structure formed with a flame extinction zone length of 1246.1 mm, and in the O_1:O_2=1:9 process, the stability of the high-temperature flame structure was relatively poor, with the longest flame extinction zone of all four processes, reaching 1561.3 mm. Compared to the pure oxygen combustion process, the flame extinction zone length was reduced by 56.5% in the O_1:O_2 =3:7 process with oxygen-enriched combustion. This demonstrates that the O_1:O_2=3:7 oxygen-enriched combustion process can effectively optimize the high-temperature flame structure, compensating for the instability in the flame structure in the staged combustion process.

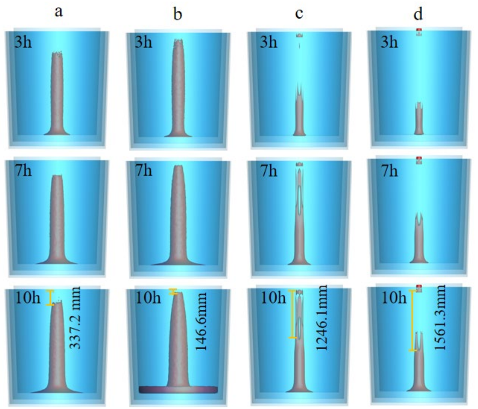

Fig. 15. Flame shape structure at 1400 K. a:Pure oxygen combustion support; b:$O_1:O_2=3:7$; c:$O_1:O_2=2:8$; d:$O_1:O_2=1:9$

3) The impact of primary air velocity on the temperature field inside the furnace

Figure 16 reveals the temperature contour maps inside the steel ladle furnace under four different processes. It can be observed that with the progression of the baking time, the high-temperature flame area gradually increases and reaches its maximum at the end of the process. By observing the high-temperature flame area under the $O_1:O_2=3:7$ process, it is seen to align with the pure oxygen combustion process. As the fuel and oxygen are rapidly injected into the ladle through the nozzle, there is a certain difference in the location where each process forms a stable high-temperature flame. At the end of the 10-hour baking process, the distance between the stable flame formation and the nozzle for each process is as follows: 1567.8 mm (pure oxygen combustion), 1178.1 mm ($O_1:O_2=3:7$), 2129.7 mm ($O_1:O_2=2:8$), and 2175.0 mm ($O_1:O_2=1:9$). The $O_1:O_2=3:7$ process, using staged combustion with oxygen, forms a stable high-temperature flame more quickly compared to other processes. The distance to form a stable high-temperature flame is shortened by 389.7 mm compared to the pure oxygen combustion process, further confirming that when using $O_1:O_2=3:7$, the drawbacks of lower combustion temperature in staged combustion are effectively compensated.

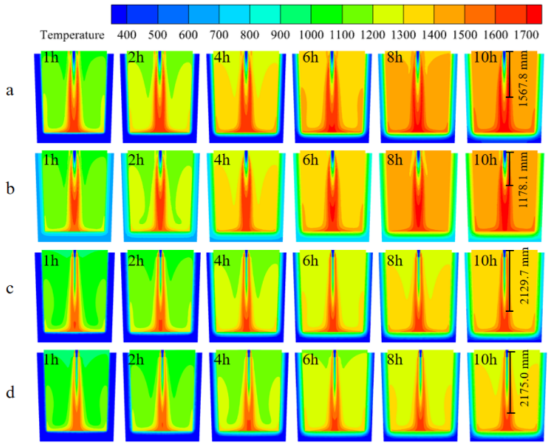

Fig. 16.Temperature field in the ladle. a:Pure oxygen combustion support; b:$O_1:O_2=3:7$; c:$O_1:O_2=2:8$; d:$O_1:O_2=1:9$

Figure 17 presents the temperature contour maps of the steel ladle inner wall under the four processes: pure oxygen staged combustion and pure oxygen combustion. As the baking process progresses, the temperature from the working layer to the insulation layer of the ladle gradually increases. By the end of the baking, the inner wall temperature of the ladle exceeds 1200 K under all four processes. A closer analysis of the local regions shows that under the $O_1:O_2=3:7$ process, the temperature on the inner wall of the ladle exhibits a significant temperature gradient in the depth direction. The temperature fluctuation within the refractory material of the ladle wall is minimal, and a broad high-temperature zone is formed within a certain thickness range. This characteristic indicates that under the pure oxygen staged combustion process ($O_1:O_2=3:7$), the high-temperature flame is rigid and provides a stable heat source, which facilitates efficient heat conduction and uniform distribution along the ladle wall. From the perspective of the steel ladle inner wall temperature distribution, it is confirmed that the $O_1:O_2=3:7$ staged combustion process strengthens the stability of heat transfer. This provides effective theoretical support for the selection and optimization of ladle baking process technologies.

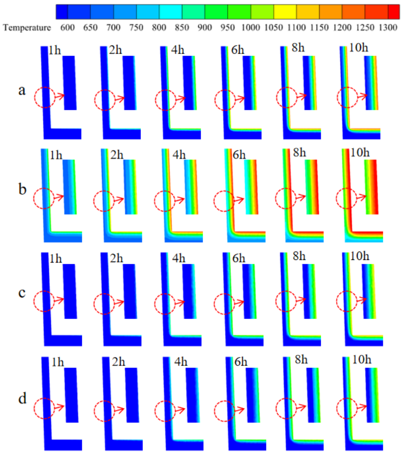

Fig. 17. Temperature distribution of the ladle wall. a:Pure oxygen combustion support; b:$O_1:O_2=3:7$; c:$O_1:O_2=2:8$; d:$O_1:O_2=1:9$

Figure 18 analyzes the temperature variation characteristics of four monitoring points under different primary air speeds. It can be observed that under the $O_1:O_2=3:7$ process, the temperature at each monitoring point is significantly higher than in the other processes. The temperature at the d5 monitoring point under pure oxygen combustion is the lowest, while the temperature at the d2 monitoring point under the three pure oxygen staged combustion processes is the lowest. Calculations show that the average temperature of the monitoring points for the pure oxygen combustion process is 1295.3 K, while the average temperature of the monitoring points for the $O_1:O_2=3:7$ process is 1429.4 K, which is 134.1 K higher than that of the pure oxygen combustion process. A comparative analysis of the average temperatures at the monitoring points for the three pure oxygen staged combustion processes reveals that the $O_1:O_2=3:7$ process increases the temperature by 31.1% and 35.3% compared to the $O_1:O_2=2:8$ and $O_1:O_2=1:9$ processes, respectively. This demonstrates that the $O_1:O_2=3:7$ process can effectively compensate for the negative effects brought by the pure oxygen staged combustion technology, optimizing the inner wall temperature distribution and providing a key basis for thermal optimization in ladle baking processes.

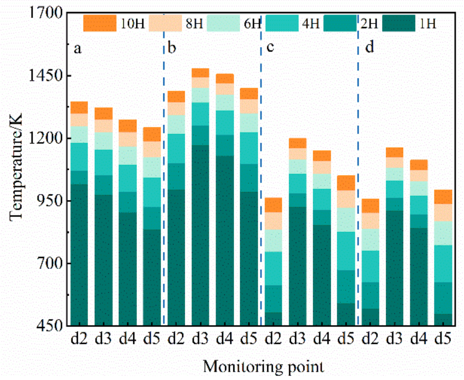

Fig. 18. Temperature changes at monitoring points. a:Pure oxygen combustion support; b:O_1:O_2=3:7; c:O_1:O_2=2:8; d:O_1:O_2=1:9

Figure 19 presents the dynamic temperature evolution at the bottom of the ladle under the four processes of pure oxygen combustion and pure oxygen staged combustion. During the early stage of baking, the temperatures at the bottom of the ladle for all four processes are at a relatively low level, gradually increasing as the baking time progresses. After 1 hour, the temperature at the bottom of the ladle for the pure oxygen combustion process reaches 1300 K, while for the pure oxygen staged combustion processes (O_1:O_2=3:7, 2:8, 1:9), the temperatures are 1300 K, 1200 K, and 1200 K, respectively. At the end of 10 hours of baking, the bottom temperatures for all four processes reach 1500 K. Notably, for the O_1:O_2=2:8 and O_1:O_2=1:9 processes, the bottom temperature increases at a faster rate throughout the entire baking process. Such a rapid temperature rise could lead to thermal stress concentration on the bottom refractory bricks, accelerating material degradation and adversely affecting their service life. In contrast, the temperature rise for the O_1:O_2=3:7 process is more gradual, which, while still meeting the baking requirements, helps protect the refractory bricks and extends their lifespan. This provides a theoretical basis for process optimization and equipment maintenance.

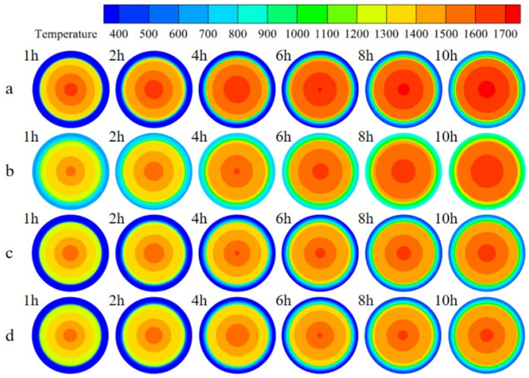

Fig. 19. Temperature nephogram at the bottom of the ladle. a:Pure oxygen combustion support; b:O_1:O_2=3:7; c:O_1:O_2=2:8; d:O_1:O_2=1:9

To systematically analyze the temperature change rate at the bottom of the ladle, Figure 20 examines the radial temperature distribution at the bottom of the ladle for the four baking processes at three characteristic times: 3 h, 7 h, and 10 h. The results show that the bottom temperature for the pure oxygen combustion process and the pure oxygen staged combustion O_1:O_2=3:7 process is significantly higher throughout the baking process compared to the O_1:O_2=2:8 and O_1:O_2=1:9 processes. This difference is directly related to the stability of the high-temperature flame structure (as analyzed in Figure 15). Specifically, for the pure oxygen combustion process, the average temperature at the bottom of the ladle is 1394.1 K at 3 h, increasing to 1548.6 K at the end of 10 h, with an average temperature rise rate of 22 K/h. For the O_1:O_2=3:7 process, the average bottom temperature reaches 1467.2 K at 3 h, rising to 1592.3 K at the end of 10 h, with an average temperature rise rate of 17.9 K/h, which is 18.6% lower than that of the pure oxygen combustion process. The lower heating rate can effectively alleviate the thermal stress concentration caused by rapid thermal shock on the bottom refractory bricks, reduce the risk of material cracking and spalling, and extend the service life of the lining. These findings highlight the significant importance of optimizing the staged combustion air ratio for the durability of equipment, providing design parameters that support the engineering application of ladle baking processes.

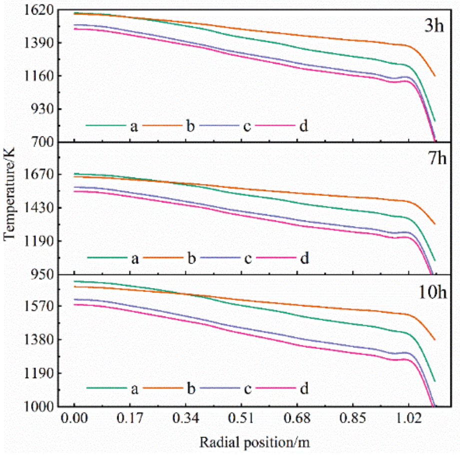

Fig. 20. Radial temperature variation at the bottom of the ladle. a:Pure oxygen combustion support; b:O_1:O_2=3:7; c:O_1:O_2=2:8; d:O_1:O_2=1:9

4) The impact of secondary air velocity on NOx concentration

The use of staged combustion technology can effectively reduce the formation of NO_x during combustion [23]. Figure 21 systematically reveals the NO_x mass concentration distribution at different interfaces for the four processes. The research shows that staged combustion technology significantly inhibits the generation and emission of NO_x. Under the pure oxygen staged combustion O_1:O_2=3:7 process, the average NO_x mass concentration reaches 3.5, which, although being the peak value among the staged combustion processes, still achieves a 46.1% reduction compared to the pure oxygen combustion process (with an average mass concentration of 6.5). Further analysis reveals that the O_1:O_2=2:8

and O_1:O_2=1:9 processes, while showing better NO_x reduction, have lower furnace temperatures (⩽1400 K) and insufficient high-temperature flame rigidity, making them unable to meet the steel shell baking requirements for thermal efficiency and temperature uniformity. Therefore, these conditions were not selected for further detailed study. The results of this study indicate that the O_1:O_2=3:7 air supply ratio demonstrates a comprehensive advantage in balancing combustion efficiency, temperature field stability, and NO_x emission control.

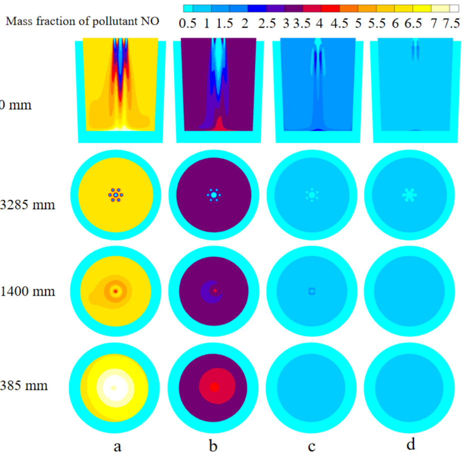

Fig. 21. NOx concentration distribution in different sections. a:Pure oxygen combustion support; b:O_1:O_2=3:7; c:O_1:O_2=2:8; d:O_1:O_2=1:9

Figure 22 systematically presents the radial distribution characteristics of NO_x mass concentration at the flue gas outlet (Y=3285 mm) and steel shell bottom (Y=385 mm) for the four processes. At the flue gas outlet section, the NO_x concentration for the pure oxygen combustion process and the pure oxygen staged combustion process with a 3:7 air supply ratio shows significant fluctuations, while the concentration curves for the pure oxygen staged combustion processes with O_1:O_2=2:8 and O_1:O_2=1:9 air supply ratios are relatively smooth. The specific data shows that the average NOx mass concentration at the flue gas outlet for the pure oxygen combustion process is 5.3, whereas for the O_1:O_2=3:7 ratio process, it drops to 2.9, a reduction of 45.2%. At the steel shell bottom section, the average NOx mass concentration for the O_1:O_2=3:7 process is reduced by 49.2% compared to the pure oxygen combustion process, demonstrating a stronger NO_x suppression effect. The above results indicate that, under the premise of ensuring high-temperature flame rigidity and meeting the required baking temperature, the O_1:O_2=3:7 pure oxygen staged combustion air supply ratio effectively suppresses the formation path of thermal NO_x by regulating the oxygen concentration distribution in the combustion region. This process not only maintains the thermal efficiency of the steel shell baking but also achieves a significant reduction in NO_x emissions, providing key technical support and an engineering application model for energy-saving and emission-reduction transformations in steel shell baking processes in the steel industry.

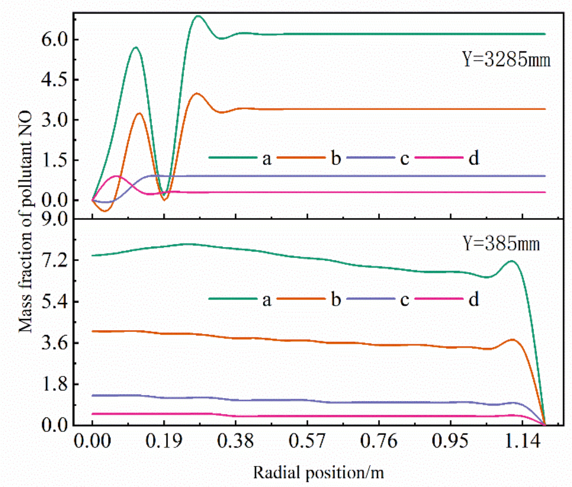

Fig. 22. Radial distribution of NOx concentration. a:Pure oxygen combustion support; b:O_1:O_2=3:7; c:O_1:O_2=2:8; d:O_1:O_2=1:9

4. Conclusion

This study developed a three-dimensional numerical model specifically for the steel ladle baking process, engaging in a comprehensive discussion of the combustion characteristics associated with both pure oxygen staged combustion technology and pure oxygen combustion technology within this context. Building upon the foundation of pure oxygen staged combustion, an optimization of the primary and secondary oxygen air-fuel ratios was undertaken. Through rigorous analysis of the combustion temperature field, flow field, high-temperature flame structure, and NOx concentration distribution, the following pivotal conclusions were derived:

1) By controlling the primary and secondary oxygen air-fuel ratio at 3:7, the pure oxygen staged combustion process adeptly addresses the temperature decay shortcomings inherent in traditional staged combustion technology. Numerical Simulation date underscores that, with this specific ratio, the overall temperature within the steel ladle furnace surpasses 1500 K, closely mirroring the temperatures achieved in pure oxygen combustion. This ratio not only mitigates the risk of localized overheating typically encountered in a pure oxygen environment but also bolsters flame stability, ensuring sustained and efficient heat release.
2) When the O_1:O_2=3:7 ratio is applied, the high-temperature flame at 1400 K inside the steel ladle exhibits a "robust and highly rigid" characteristic, with the swirl zone area effectively controlled through staged oxygen supply. This structural optimization enhances the circulation rate of the high-temperature flue gas, with the axial flow speed reaching 21 m/s and the bottom impact speed around 8.5 m/s, significantly improving the convective heat transfer efficiency.
3) The ratio of O_1:O_2 =3:7 markedly enhances the temperature distribution across the inner wall of the steel ladle. Specifically, the average wall temperature experiences an augmentation of 134.1 K when compared to the pure oxygen

combustion process. The temperature gradient exhibits a smooth progression along the depth direction of the refractory material, thereby circumventing the concentration of localized thermal stresses. Notably, the maximum temperature discrepancy between the center and the edge of the steel ladle bottom diminishes by 265.5 K in comparison to the pure oxygen combustion process. Additionally, the average heating rate of 17.9 K/h represents an 18.6% decrease from the 22 K/h observed in the pure oxygen combustion process. This reduction effectively mitigates the potential for cracking and spalling of the refractory bricks, which may be induced by rapid thermal shock.

4) The pure oxygen staged combustion process exhibits remarkable efficacy in inhibiting the formation of thermal NOx by establishing a gradient of oxygen concentration within the combustion zone. Specifically, when the O_1:O_2 is set at 3:7, the average NO_x concentration within the furnace undergoes a substantial decrease of 46.1% in comparison to the pure oxygen combustion process. Furthermore, the concentrations at both the flue gas outlet and the bottom of the steel ladle witness reductions of 45.2% and 49.2%, respectively.

Acknowledgments

The authors are grateful for the financial support by Innovation and Entrepreneurship Training Program for College Students and Project of Liaoning Provincial Department of Education (JYTMS20230932).

References

[1] He, J., Liu, G., Liu, Y., Cao, Z. & Liu, J. (2025). Comparative Study on the Effect of Different Gas Types in Baking Regenerative Ladle. *Archives of Foundry Engineering*. 25(1), 75-84. DOI: 10.24425/afe.2025.153776.

[2] Deng, S., Xu, A., Yang, G. & Wang, H. (2019). Analyses and calculation of steel scrap melting in a multifunctional hot metal ladle. *Steel research international*. 90(3), 1800435, 1-10. DOI: 10.1002/srin.201800435.

[3] Wang, W., Liao, Y., Liu, J., Huang, Z. & Tian, M. (2019). Numerical simulation and optimization of staged combustion and NO_x release characteristics in precalciner. *Journal of Thermal Science*. 28(5), 1024-1034. DOI: 10.1007/s11630-019-1164-y.

[4] Wang, Y. & Zhou, Y. (2020). Numerical optimization of the influence of multiple deep air-staged combustion on the NO_x emission in an opposed firing utility boiler using lean coal. *Fuel*. 269, 116996, 1-13. DOI: 10.1016/j.fuel.2019.116996.

[5] Munir, S., Nimmo, W. & Gibbs, B.M. (2011). The effect of air staged, co-combustion of pulverised coal and biomass blends on NO_x emissions and combustion efficiency. *Fuel*. 90(1), 126-135. DOI: 10.1016/j.fuel.2010.07.052.

[6] Zhang, J.X. & Zhang, J.F. (2016). Analysis of chemical reaction kinetics behavior of nitrogen oxide during air-staged combustion in pulverized boiler. *Bulletin of Chemical Reaction Engineering and Catalysis*. 11(1), 100-108. DOI: 10.9767/bcrec.11.1.431.100-108.

[7] Poraj, J., Gamrat, S., Bodys, J., Smolka, J. & Adamczyk, W. (2016). Numerical study of air staging in a coke oven heating system. *Clean Technologies and Environmental Policy*. 18(6), 1815-1825. DOI: 10.1007/s10098-016-1234-8.

[8] Hu, X., Zhang, J., Yu, Z., Liu, Z., Guo, J. & Xu, C. (2024). Numerical study of the combustion process in the vertical heating flue of air staging coke oven. *Processes*. 12(10), 2294, 1-19. DOI: 10.3390/pr12102294.

[9] Fan, W., Li, Y., Guo, Q., Chen, C. & Wang, Y. (2017). Coal-nitrogen release and NOx evolution in the oxidant-staged combustion of coal. *Energy*. 125, 417-426. DOI: 10.1016/j.energy.2017.02.130.

[10] Vodička, M., Hrdlička, J. & Skopec, P. (2021). Experimental study of the NO_x reduction through the staged oxygen supply in the oxy-fuel combustion in a 30 kWth bubbling fluidized bed. *Fuel*. 286, 119343, 1-9. DOI: 10.1016/j.fuel.2020.119343.

[11] Zhang, H., Zhou, P. & Yuan, F. (2021). Effects of ladle lid or online preheating on heat preservation of ladle linings and temperature drop of molten steel. *Energy*. 214, 118896, 1-11. DOI: 10.1016/j.energy.2020.118896.

[12] Zhuang, S., Zhan, D., Wang, T., Li, P. & Yang, Y. (2023). Influence of oxy-fuel lance parameters on the scrap pre-heating temperature in the hot metal ladle. *Metals*. 13(5), 847, 1-19. DOI: 10.3390/met13050847.

[13] Wang, G., Yang, F., Wu, K., Ma, Y., Peng, C., Liu, T. & Wang, L.P. (2021). Estimation of the dissipation rate of turbulent kinetic energy: A review. *Chemical Engineering Science*. 229, 116133, 1-17. DOI: 10.1016/j.ces.2020.116133.

[14] Yuan, F., Wang, H.B., Zhou, P.L. & Xu, A.J. (2018). Combustion performance of nozzles with multiple gas orifices in large ladles for temperature uniformity. *Journal of Iron and Steel Research International*. 25(4), 387-397. DOI: 10.1007/s42243-018-0048-9.

[15] Park, Y.K. & Kim, B.S. (2023). Catalytic removal of nitrogen oxides (NO, NO_2, N_2O) from ammonia-fueled combustion exhaust: A review of applicable technologies. *Chemical Engineering Journal*. 461, 141958, 1-13. DOI: 10.1016/j.cej.2023.141958.

[16] Zhou, Z., Han, X., Wang, X., Yu, J. & Shan, S. (2023). New coefficients of the weighted-sum-of-gray-gases model for gas radiation characteristics of hydrogen/natural gas blends combustion. *International Communications in Heat and Mass Transfer*. 149, 107090, 1-10. DOI: 10.1016/j.icheatmasstransfer.2023.107090.

[17] Calvo, W.A., Dignani, M.L., Galliano, P.G., Brandaleze, E. & Martínez, A.G.T. (2022). Basic slag corrosion of alumina–magnesia–carbon refractory bricks containing Al and Si antioxidants. *International Journal of Applied Ceramic Technology*. 19(4), 2331-2343. DOI: 10.1111/ijac.14017.

[18] Liu, Q., Wang, J., Liu, G. & Liu, Y. (2025). Optimized combustion characteristics in a top-blown converter utilizing a swirling-flow post-combustion oxygen lance. *Energy*. 326, 136082, 1-15. DOI: 10.1016/j.energy.2025.136082.

[19] Jiang, P. & He, X. (2020). Experimental investigation of flow field characteristics in a mixed-flow trapped vortex

combustor. *Aerospace Science and Technology*. 96, 105533, 1-11. DOI: 10.1016/j.ast.2019.105533.

[20] Giannadakis, A., Naxakis, A., Romeos, A., Perrakis, K. & Panidis, T. (2019). An experimental study on a coaxial flow with inner swirl: Vortex evolution and flow field mixing attributes. *Aerospace Science and Technology*. 94, 105373, 1-16. DOI: 10.1016/j.ast.2019.105373.

[21] Gichov, Y. & Stupak, M. (2020). An effectiveness analysis of the pulsed resonant fuel combustion in the processes of steel-casting ladle drying and warming. *Eastern-European Journal of Enterprise Technologies*. 2(8), 104, 52-59. DOI: 10.15587/1729-4061.2020.201077.

[22] Campos, M.G.G., Dos Santos, M.F., Moreira, M.H., Angélico, R.A., Sako, E.Y. & Pandolfelli, V.C. (2020). Holistic view of the insulating layer on the thermal efficiency of a steel ladle lining. *International Journal of Ceramic Engineering & Science*. 2(3), 113-129. DOI: 10.1002/ces2.10043.

[23] Li, Z., Yi, Q., Zhang, Y., Zhou, H., Zhao, Y., Huang, Y. & Hao, Y. (2020). Numerical study and design strategy for a low emission coke oven system using oxy-fuel combustion of coke oven gas. *Journal of Cleaner Production*. 252, 119656, 1-15. DOI: 10.1016/j.jclepro.2019.119656.